The Storm of Decameter Spikes During the Event of 14 June 2012

N. V. Shevchuk, V. N. Melnik, S. Poedts, V. V. Dorovskyy, J. Magdalenic, A. A. Konovalenko, A. I. Brazhenko, C. Briand, et al.

Solar Physics
A Journal for Solar and Solar-Stellar Research and the Study of Solar Terrestrial Physics

ISSN 0038-0938

Sol Phys
DOI 10.1007/s11207-015-0799-4

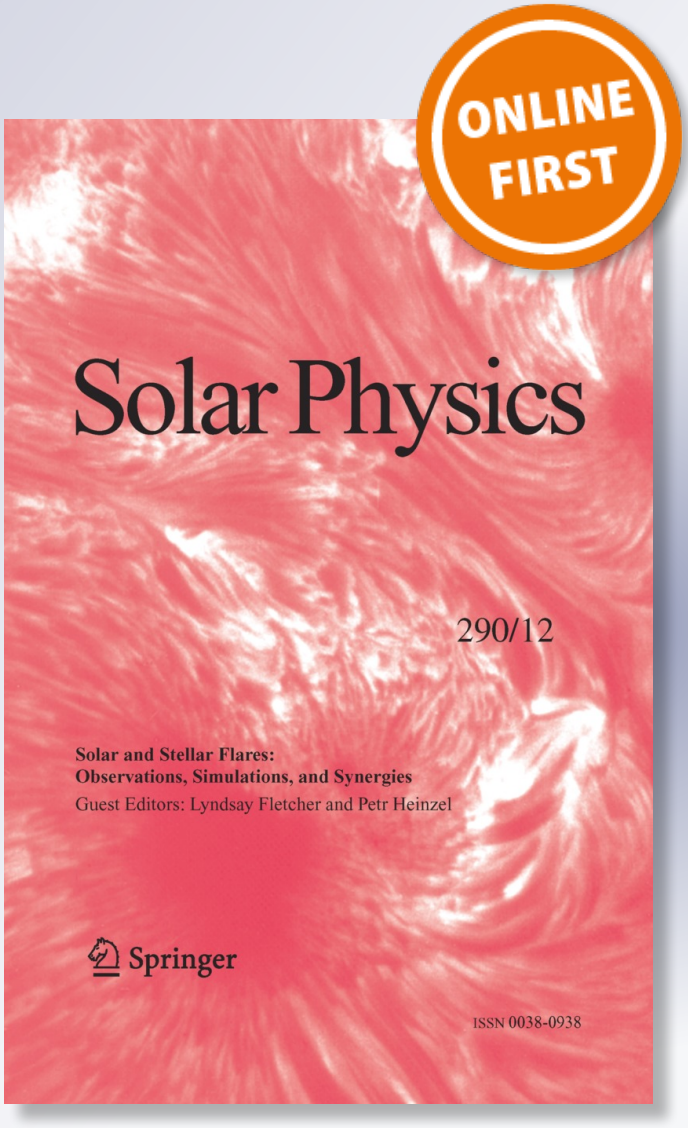

Springer

Solar Phys
DOI 10.1007/s11207-015-0799-4

The Storm of Decameter Spikes During the Event of 14 June 2012

N.V. Shevchuk[1,2] · V.N. Melnik[1] · S. Poedts[2] · V.V. Dorovskyy[1] · J. Magdalenic[3] · A.A. Konovalenko[1] · A.I. Brazhenko[4] · C. Briand[5] · A.V. Frantsuzenko[4] · H.O. Rucker[6] · P. Zarka[5]

Received: 13 February 2015 / Accepted: 6 October 2015

Abstract An event on 14 June 2012, observed with the radio telescopes UTR-2 (Kharkov, Ukraine), URAN-2 (Poltava, Ukraine), and NDA (Nançay, France) during a joint Summer campaign, is analyzed and discussed. The high solar activity resulted in a storm of spikes, and a storm of Type III bursts, Type IIIb bursts, and a Type IV burst observed in the decameter band. During the observed time interval, the average flux of radio emission changed twice. Using spikes as a tool for diagnostics of plasma parameters, we followed variations of the coronal temperature and the coronal magnetic field in the observed time interval. Thus, in frames of the model described in this article the observed decameter spikes' durations of $0.3-1$ seconds correspond to the coronal plasma temperatures of $\approx 0.1-0.6\times 10^6$ K. At the same time the spikes' frequency bandwidths of $25-80$ kHz give us the magnetic-field value of about 2 G.

✉ N.V. Shevchuk
mykola.shevchuk@rian.kharkov.ua

V.N. Melnik
Melnik@rian.kharkov.ua

S. Poedts
Stefaan.Poedts@wis.kuleuven.be

J. Magdalenic
jasmina.magdalenic@sidc.be

1 Institute of Radio Astronomy, Kharkov, Ukraine

2 Catholic University of Leuven, Leuven, Belgium

3 Observatoire de Paris, Meudon, France

4 Royal Observatory of Belgium, Brussels, Belgium

5 Institute of Geophysics, Gravimetrical Observatory, Poltava, Ukraine

6 Space Research Institute, Graz, Austria

Published online: 08 December 2015

1. Introduction

Spikes are solar radio bursts that are usually observed during high solar activity. Independently of the frequency band in which they are observed, they have short durations and narrow frequency bandwidths when compared with other solar radio bursts.

Spikes were described for the first time by De Groot (1960) and Elgaröy (1961), who observed them at 190 – 215 MHz (Elgaröy, 1961) and 274 – 390 MHz (De Groot, 1960) independently. The bursts with durations of approximately 0.1 second and with narrow bandwidths of only a few MHz were named "small bursts" or "pips". The term "spike" was first used by Takakura (1959). During the next decades spikes were observed in different bands ranging from decameters up to decimeters. Summing up the different results obtained by different authors, we can allocate the main properties of spikes:

- spikes are observed simultaneously with different types of radio bursts (Type II, III, IIIb, IV bursts);
- spike durations decrease with the increase of the observational frequency, namely from one second at frequencies 12.5 – 30 MHz (Ellis and McCulloch, 1967; Baselian *et al.*, 1974; de La Noe, 1975; Sawant, Bhonsle, and Alurkar, 1976) to 400 – 100 ms at frequencies 145 – 345 MHz (McKim Malville, Aller, and Jensen, 1967; Markeev and Chernov, 1970; Bakunin and Chernov, 1985), 155 – 36 ms at frequencies 0.3 – 2 GHz (Droege, 1977; Guedel and Benz, 1990; Dąbrowski, Rudawy, and Karlický, 2011) and less than 100 ms (instrumental resolution) at frequencies 6 – 8 GHz (Benz *et al.*, 1992);
- spike bandwidths increase with the increase of the observational frequency, *viz.* from tens of kHz at frequencies 20 – 100 MHz (Ellis and McCulloch, 1967; Warwick and Dulk, 1969; Baselian *et al.*, 1974; de La Noe, 1975) to 1.5 – 4 MHz at frequencies 100 – 300 MHz (Elgaröy, 1967; Markeev and Chernov, 1970), 10 MHz at frequency 0.8 – 2 GHz (Droege, 1977; Dąbrowski, Rudawy, and Karlický, 2011), and even up to 100 MHz at frequency 6.4 – 8.6 GHz (Benz *et al.*, 1992);
- spike frequency-drift rates vary within wide limits. At frequencies lower than 100 MHz, the spikes drift rates are small (20 – 150 kHz s^{-1}) or practically zero (Ellis and McCulloch, 1967; Warwick and Dulk, 1969; Baselian *et al.*, 1974; de La Noe, 1975). At meter range, Tarnstrom and Philip (1972) separated spikes into three groups, depending on their drift rates. According to these authors, there are fast-drifting spikes with drift rates higher than 100 MHz s^{-1} (first group), intermediate-drifting spikes with rates lower than 100 MHz s^{-1} (second group), and spikes without noticeable drift rates (third group). At frequencies 0.8 – 2 GHz, spikes with positive and negative drift rates were observed. The extreme values were equal to 1608 MHz s^{-1} and 776 MHz s^{-1} (Dąbrowski, Rudawy, and Karlický, 2011), respectively;
- the spike fluxes in most cases are not higher than 100 s.f.u. (where 1 s.f.u = 10^{-22} W m^{-2} Hz^{-1}) (Benz *et al.*, 1992; Melnik *et al.*, 2014). The maximum value of spike flux registered in the decameter range was equal about 200 s.f.u. (Melnik *et al.*, 2014). The brightness temperatures of spikes can reach $10^{12} - 10^{15}$ K, which points to a non-thermal mechanism of radiation (Messerotti, Nonino, and Zlobec, 1985; Benz, 1986);
- the polarization of the spikes in most cases is circular and varies from 0 to 100 % (Markeev and Chernov, 1970; Barrow and Saunders, 1972; Benz, Csillaghy, and Aschwanden, 1996). The average value is only 25 % (Benz, 1986);
- two mechanisms of spike generation are considered: the electron-cyclotron maser mechanism and the plasma mechanism. The electron-cyclotron maser mechanism is considered to describe high-frequency spikes (Benz *et al.*, 1992; Fleishman and Mel'nikov, 1998), while the plasma mechanism is involved to describe low-frequency ones (Warwick and

Dulk, 1969; Baselian *et al.*, 1974; Stewart, 1975; Zhelezniakov and Zaitsev, 1975; de La Noe, 1975; Melnik *et al.*, 2014).

Following Melnik *et al.* (2014), the decameter bursts with the short durations of about one second and narrow frequency bandwidths 50 – 70 kHz chaotically located on the dynamical spectrum we call decameter spikes (Figure 1). These morphological properties of the spikes make their identification simple and confident.

In this article, the analysis of spikes observed simultaneously with the storm of Type III bursts and Type IV burst is presented. The studied event was observed in a continuous frequency band 8 – 42 MHz on 14 June 2012 with the radio telescopes UTR-2 (Ukrainian T-shaped Radio telescope, second modification, Kharkov, Ukraine), URAN-2 (Ukrainian Radio interferometer of Academy of Science, Poltava, Ukraine), and NDA (Nançay Decameter Array, Nançay, France). The main parameters of the spikes (*i.e.* their durations, bandwidths, and fluxes) and their dependencies on the frequency are obtained. Assuming that spike durations and bandwidths are defined by the coronal plasma parameters (such as temperature and magnetic field), we traced how these coronal parameters changed during the day of observations.

The article is arranged as follows. In Section 2 we describe the technique and equipment used for the observations. In Section 3 we provide the results of the analysis of the spikes observational properties such as duration, frequency, decay time, bandwidth, *etc.* Finally, in Section 4 we discuss how the spike parameters depend on the ambient plasma properties. The information obtained is then used to derive the temperature and magnetic field of the plasma in which the spikes have been generated.

2. Observations

2.1. Instrumentation

During the Summer campaign of observations in 2012, three radio telescopes, *viz.* UTR-2 (Kharkov, Ukraine), URAN-2 (Poltava, Ukraine), and NDA (Nançay, France), were used simultaneously. Only four sections of the UTR-2 radio telescope, with an effective area of about 50,000 m^2, were used (Braude and Men', 1996). The effective areas of URAN-2 and NDA radio telescopes are 28,000 m^2 and 2×4000 m^2 correspondingly (Boischot *et al.*, 1980; Megn *et al.*, 2003). The radio telescopes UTR-2 and URAN-2 were equipped with a new Digital Spectra Polarimeter of Z-modification (DSP-Z: Ryabov *et al.*, 2010). The observations were carried out in the frequency band 8 – 32 MHz with high time (100 ms) and frequency (4 kHz) resolution. The registrations with the radio telescope NDA, on the other hand, were carried out in the frequency band 28 – 42 MHz. As a recording unit the spectrometer ROBIN (ROBust receiver) with time (37 ms) and frequency (12 kHz) resolution was used (Weber *et al.*, 2005). The simultaneous use of these tools gave us the opportunity to carry out observations in a continuous frequency band ranging from 8 to 42 MHz with an overlap in the bandwidth 28 – 32 MHz (see Figures 1, 2).

From these figures (Figures 1, 2) it is clearly visible that the number of spikes in the frequency range 8 – 32 MHz is significantly greater than in the range 28 – 42 MHz. This is related with the fact that the UTR-2 radio telescope sensitivity is more than one order of magnitude higher than the sensitivity of NDA radio telescope. For instance, the UTR-2 and NDA radio telescopes sensitivities at frequency 25 MHz, recalculated for the hardware parameters of the experiment (effective area, time, and frequency resolution), are 300 Jy

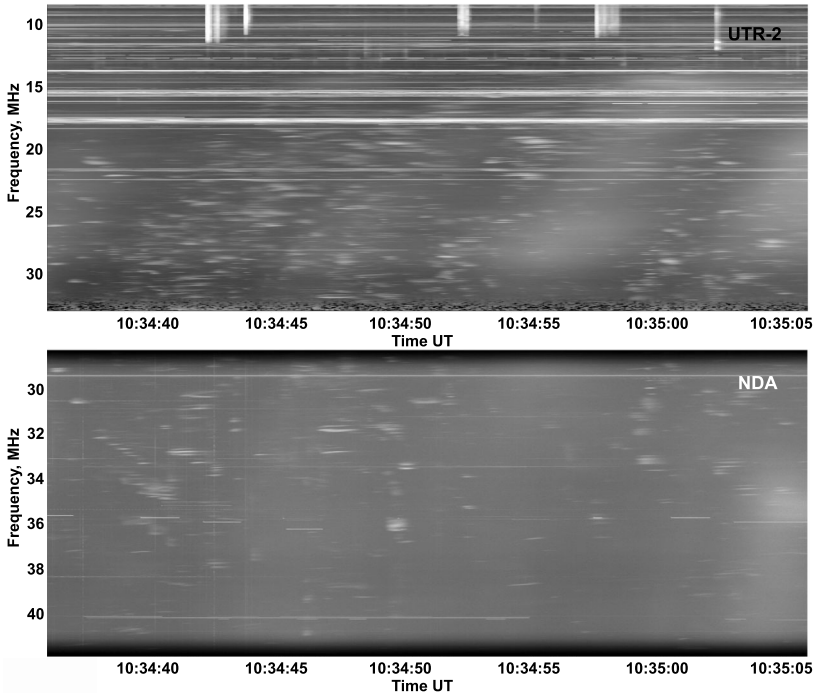

Figure 1 The dynamical spectrum in the frequency range 8 – 42 MHz. The upper part corresponds to the data obtained with the UTR-2 radio telescope and the lower one to data obtained with the NDA radio telescope.

and 6000 Jy, respectively. Moreover, the real NDA sensitivity may be even lower since the measured signal travels from the array to register unit (ROBIN) through a 1-kilometer fiber optic line, which apparently leads to signal loss and to decrease of the signal-to-noise ratio.

2.2. Event on 14 June 2012

An interesting event was recorded on 14 June 2012 04:45 – 16:00 UT. A storm of spikes was observed simultaneously with the storm of Type III bursts and a Type IV continuum (Figure 3a). This high activity is possibly related to the group of sunspots (NOAA 11504 – 11508) observed in the central part of the solar disk, South of the Equator (see Figure 4a). The image was obtained with the *Solar and Heliospheric Observatory spacecraft* (SOHO) in the 304 Å ultraviolet band of the *Extreme ultraviolet Imaging Telescope* (EIT: soho.nascom.nasa.gov). Also on this day, a Coronal Mass Ejection (CME) was observed with the *Solar-Terrestrial Relations Observatory* spacecraft (STEREO) (stereo-ssc.nascom.nasa.gov); see Figure 4b.

During the observations the average flux of radio emission changed twice (Figure 3b). Such variations of average flux can be related to the changes of the coronal plasma parameters. In the framework of the hypotheses that the durations of spikes are determined by the temperature of the ambient plasma and that their bandwidths are determined by the magnetic field in the ambient plasma, we checked whether the plasma parameters varied during the day. Hence, the observations were conventionally divided into three time intervals.

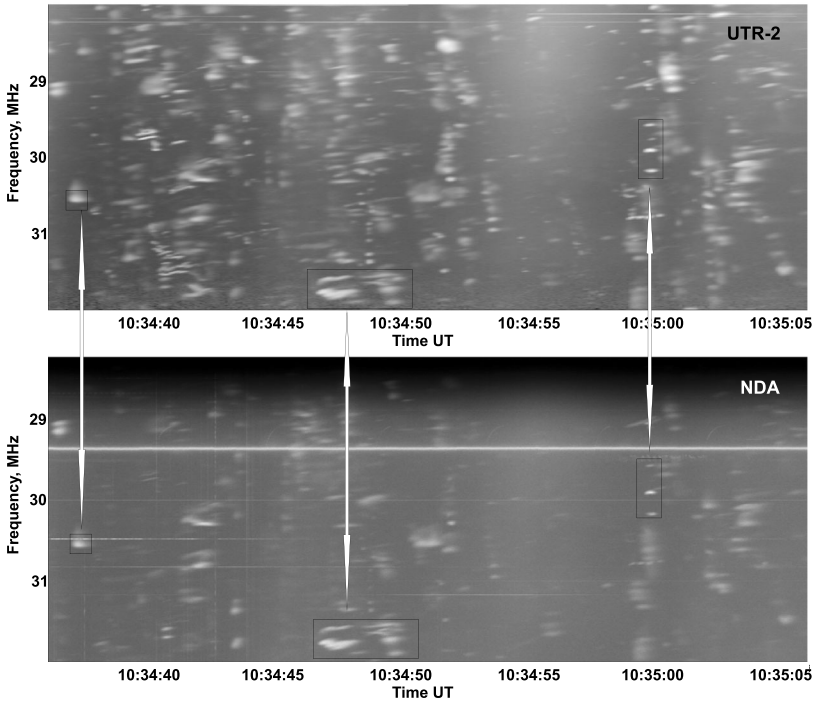

Figure 2 The dynamical spectrum in the frequency range 28 – 32 MHz. The upper part corresponds to the data obtained with the UTR-2 radio telescope and the lower one to data obtained with the NDA radio telescope.

During the first time interval, which lasted for five hours, namely from approximately 4:45 – 9:45 UT, the storm of spikes was observed simultaneously with the storm of Type III bursts (11 bursts per minute). In this time interval the average flux was about 300 s.f.u. (Figure 3b).

From approximately 9:45 – 13:30 UT (the second time interval) the flux decreased to approximately 100 s.f.u., which on the dynamical spectrum corresponded to a decrease in the number of Type III bursts to five bursts per minute. At the same time, the storm of spikes continued.

The third time interval started at 13:30 UT with an increase of the flux to a few thousands of s.f.u. This flux increase on the dynamical spectrum shows up as a Type IV burst. The start time of the Type IV continuum practically coincides with the start time of the CME that was observed on this day (Figure 4b). The storm of spikes ceased after half an hour, after the Type IV burst has started. The Type IV burst itself lasted for about two hours.

It is necessary to mention that during the first time interval the storm of spikes was observed within the full frequency band 8 – 42 MHz. However, during the second and third time intervals, spikes were observed only in the frequency bands 10 – 42 MHz and 13 – 42 MHz, respectively. For each time interval a considerable number of spikes were analyzed. For the first time interval we measured more than 500 spikes, for the second time interval more than 800, and for the third interval more than 300 spikes. The spike parameters were measured manually using temporal and frequency profiles of the bursts. Examples of such profiles are shown in Figures 5 and 6 and marked by the arrows.

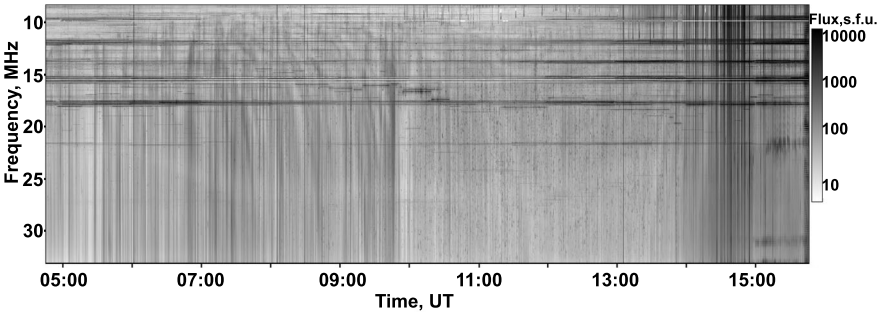

a)

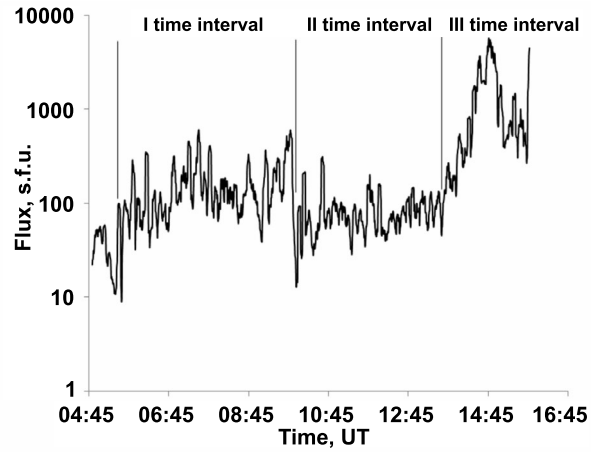

b)

Figure 3 The dynamical spectrum (a) and time profile (b) obtained with URAN-2 (full day of observations).

3. Analysis of the Observations

As mentioned earlier, spikes have short durations in all frequency bands. A typical example of a spike temporal profile is presented on Figure 5. In the majority of cases the temporal profiles of spikes are not symmetrical. The decay phase of the burst is somewhat longer than the rise phase. On such profiles at half maximum flux, the rise time [τ_r], the decay time [τ_d], and the total duration [$d = \tau_r + \tau_d$] were measured.

In Figures 7, 8, and 9 the histograms showing distributions of spikes duration for each of three time intervals at different frequencies are presented. From Figure 7 it is clear that the range of spike durations shows only small variations with frequency during the first time interval. The majority of bursts have durations of 0.4 – 1 seconds.

At the same time, the histograms for the second and third time intervals (Figures 8, 9) show a shift of the distribution maximum with the frequency, from a region of longer durations (0.8 – 1 seconds) to the region of shorter durations (0.3 – 0.5 seconds). These variations of durations with frequency are clearly visible in Figure 10, which displays the spike average duration dependencies *versus* the frequency for the first (a), second (b), and third (c) time intervals.

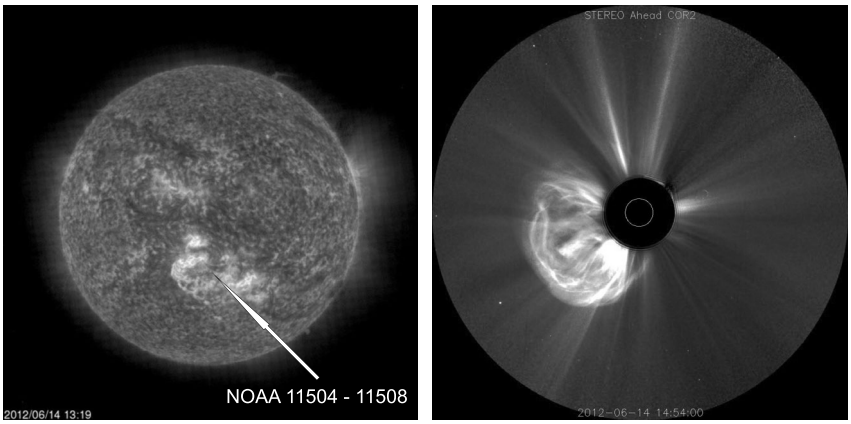

Figure 4 The group of spots (NOAA 11504 – 11508) on the solar disk (a) and coronal mass ejection (b).The images were obtained with SOHO and STEREO (ahead) spacecrafts.

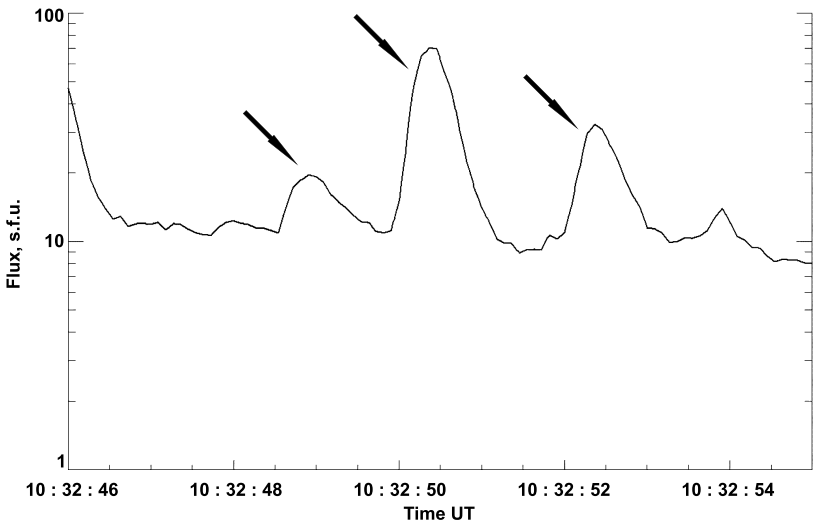

Figure 5 An example of the spike temporal profiles at frequency of 24.38 MHz (data obtained with UTR-2).

The average values of spike duration [d], rise time [τ_r], and decay time [τ_d] at one particular frequency differ from one interval to another during the day (Table 1). Starting from certain frequencies (21 – 22 MHz) the average values of durations, and as a consequence also the rise and decay times, decreased during the day. In most cases (80 %) the average value of the rise time is shorter than that of the decay time, which is also visible from the time profiles of the first two spikes in Figure 5.

3.1. Decay Time

The dependencies of the spike decay time on frequency for all three temporal intervals are presented in Figure 11. We did not find any specific dependence of the decay time on fre-

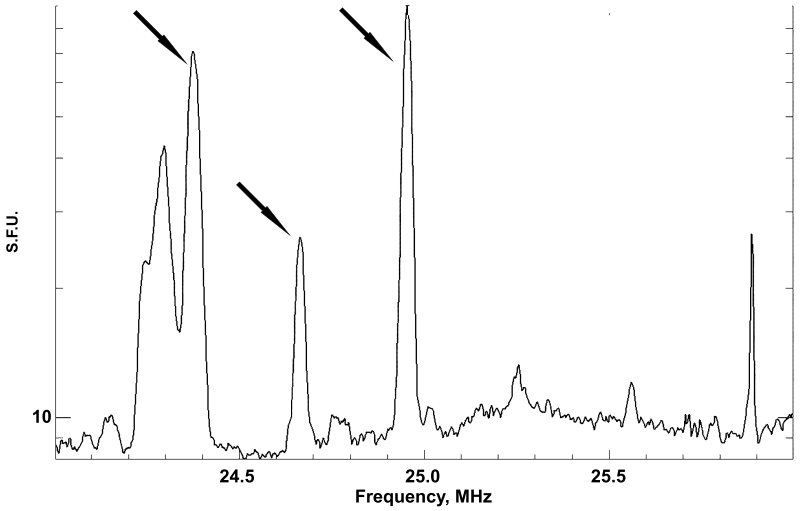

Figure 6 The frequency profile of spikes at 10:32:52 UT (data obtained with UTR-2).

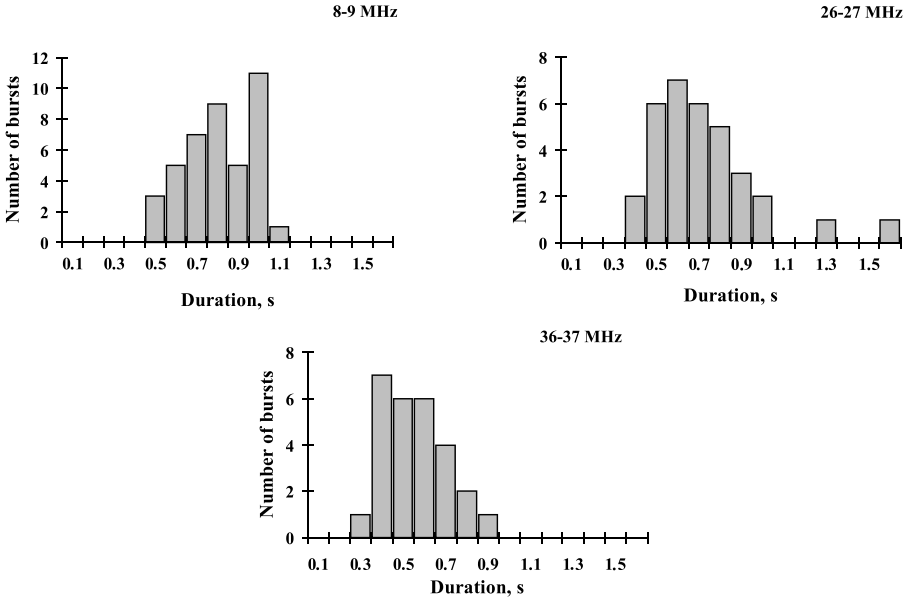

Figure 7 Histograms of spike distributions by duration for the first temporal interval at different frequencies.

quency for the first time interval (Figure 11a), similarly to the total-duration dependence in this interval (Figure 10a). The dependencies for the second and third intervals (Figure 11b, c), however, can be approximated by a power-law in the form of $\tau_{\rm d} \sim f^{p}$ using the least-squares method. The power-law indices $[p]$ are close to -1, having values of -1.01 and -1.05 for the second and third time interval, respectively. For comparison of dependen-

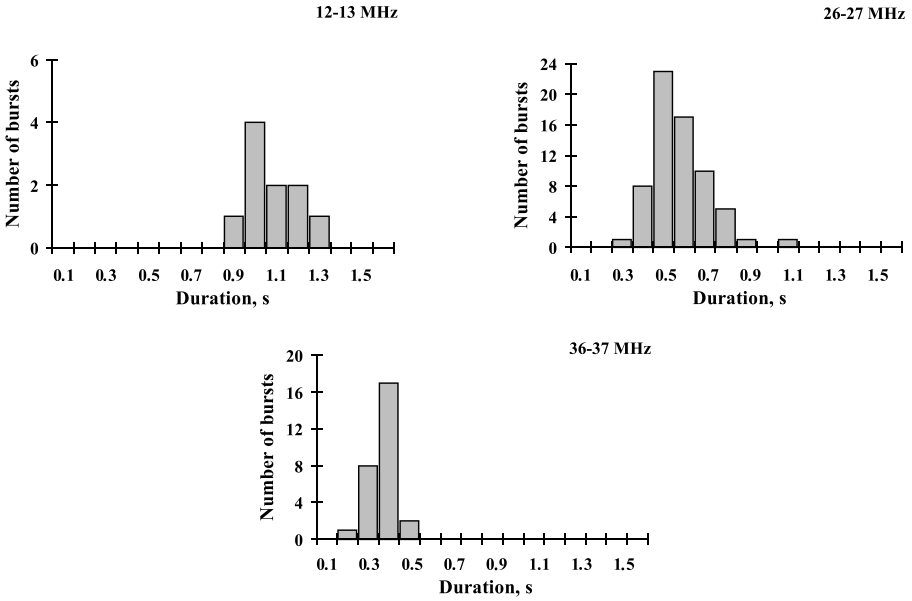

Figure 8 Histograms of spike distributions by duration for the second temporal interval at different frequencies.

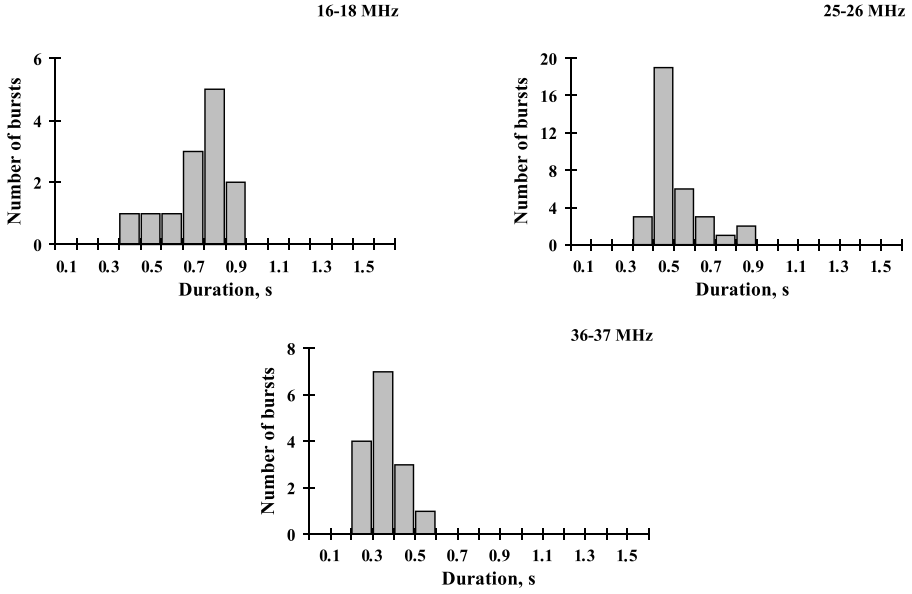

Figure 9 Histograms of spike distributions by duration for the third temporal interval at different frequencies.

cies and for further calculations we use the approximation $\tau_d = bf^{-1}$. The coefficient $[b]$ for the second temporal interval is about 7.6 and for the third interval is approximately 6.4. Al-

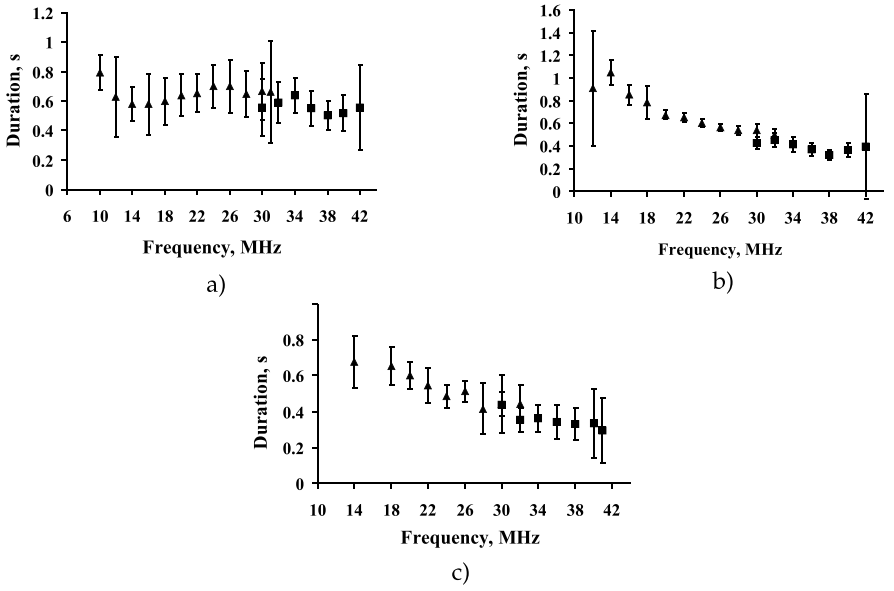

Figure 10 The spike average duration *versus* frequency for the first (a), second (b), and third (c) temporal intervals. The triangles correspond to data obtained with the UTR-2 radio telescope and squares to data obtained with the NDA radio telescope.

Table 1 The variations of duration [d], rise [τ_r] and decay [τ_d] times at frequencies 25 MHz (UTR-2) and 35 MHz (NDA)

Radio telescope	Parameter	Temporal interval		
		I	II	III
UTR-2	d [s]	0.77 ± 0.14	0.54 ± 0.05	0.47 ± 0.2
NDA		0.58 ± 0.15	0.39 ± 0.09	0.32 ± 0.13
UTR-2	τ_r [s]	0.35 ± 0.07	0.27 ± 0.05	0.2 ± 0.03
NDA		0.25 ± 0.06	0.19 ± 0.05	0.18 ± 0.08
UTR-2	τ_d [s]	0.42 ± 0.1	0.27 ± 0.06	0.27 ± 0.2
NDA		0.33 ± 0.12	0.2 ± 0.05	0.14 ± 0.07

though these two dependencies are similar, the dependence for the third interval lies slightly lower than the dependence for the second interval.

According to McKim Malville, Aller, and Jensen (1967) and Benz (1986), the decay time of spikes [τ_d] is comparable with the damping time of Langmuir waves in plasma [τ_{coll}]. The latter is determined by the temperature of the ambient plasma as follows:

$$\tau_{coll} = \frac{1}{n\sigma V_{Te}} = \frac{k_B^{3/2}}{\pi^2 e^2 m^{1/2} Z_1^2 Z_2^2 \lambda} \frac{T^{3/2}}{f^2}, \quad (1)$$

where n denotes the plasma density, $\sigma = \pi\lambda Z_1^2 Z_2^2 e^4/m^2 V_{Te}^4$ denotes the transport cross-section, λ is the Coulomb logarithm, V_{Te} is the electron thermal velocity, e is the electron charge, m is the electron mass, T is the temperature, and f is the frequency.

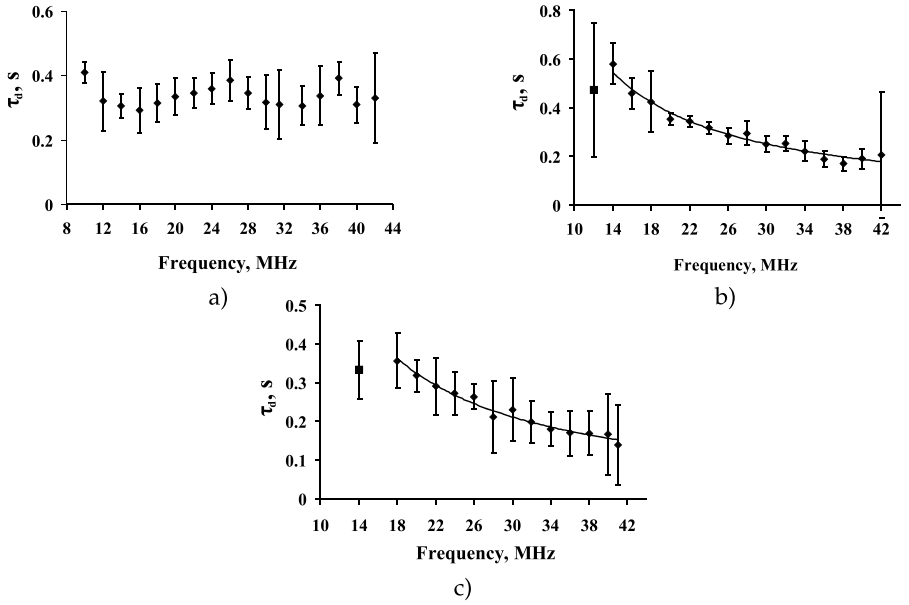

Figure 11 The dependencies of average values τ_d on frequency for the first (a), second (b), and third (c) time intervals.

As a consequence, if $\tau_d \approx \tau_{coll}$, then, knowing the spike decay time and using Equation (1), we can estimate the temperature of the coronal plasma at the distance from the Sun that corresponds to each observing frequency. Taking into account that $Z_1 = Z_2 = 1.06$, $\lambda = 18.8$ (Guedel and Benz, 1990) the expression for the determination of coronal temperature can be written as

$$T = 8 \times 10^3 f^{4/3} \tau_{coll}^{2/3}, \tag{2}$$

where f denotes the frequency in MHz and τ_{coll} denotes collision time in seconds. The obtained values and dependencies of the temperature $[T]$ *versus* the frequency for all temporal intervals are presented in Figure 12 and in Table 2.

The results obtained show that the temperature $[T]$ is rising when the frequency is increasing, as can be expected. However, the values obtained for the temperature $[T]$ are considerably smaller than the usually considered coronal plasma temperature (of the order of 10^6 K) at the distances corresponding to the decameter range.

Therefore, we inspected the correspondence of the coronal temperatures obtained with the high-frequency spikes (362 – 1010 MHz) (Guedel and Benz, 1990) and the low-frequency spikes (8 – 42 MHz). In order to do so, we put the empirically found dependence $\tau_d = bf^{-1}$ into Equation (2) (similarly to what was done by Guedel and Benz (1990)) and thus obtained the following dependence $[T(f)]$:

$$T(f) \approx 4 \times 10^4 f^{2/3}. \tag{3}$$

Then we built the dependence of temperature on the frequency for a wide frequency range, *viz.* from 8 MHz to 1010 MHz, and plotted the temperatures obtained in both cases (Figure 13).

These temperatures are in good agreement with the dependence found in Equation (3). Hence, we conclude that if the decay time is considered to be defined by the particle collision

Table 2 The variation of the plasma temperature during the observational day

f [MHz]	n_e [10^6 cm^{-3}]	Temporal interval		
		I	II	III
		T [10^6 K]	T [10^6 K]	T [10^6 K]
10	1.2	0.1 ± 0.02	–	–
14	2.4	0.13 ± 0.03	0.19 ± 0.06	0.13 ± 0.05
18	4	0.18 ± 0.06	0.22 ± 0.09	0.2 ± 0.07
22	6	0.25 ± 0.07	0.25 ± 0.04	0.23 ± 0.09
26	8.4	0.34 ± 0.1	0.28 ± 0.07	0.27 ± 0.07
30	11	0.36 ± 0.15	0.31 ± 0.08	0.3 ± 0.15
34	14.3	0.42 ± 0.14	0.34 ± 0.1	0.3 ± 0.12
38	17.9	0.58 ± 0.15	0.33 ± 0.09	0.33 ± 0.16
42	21.8	0.59 ± 0.3	0.43 ± 0.5	0.32 ± 0.26

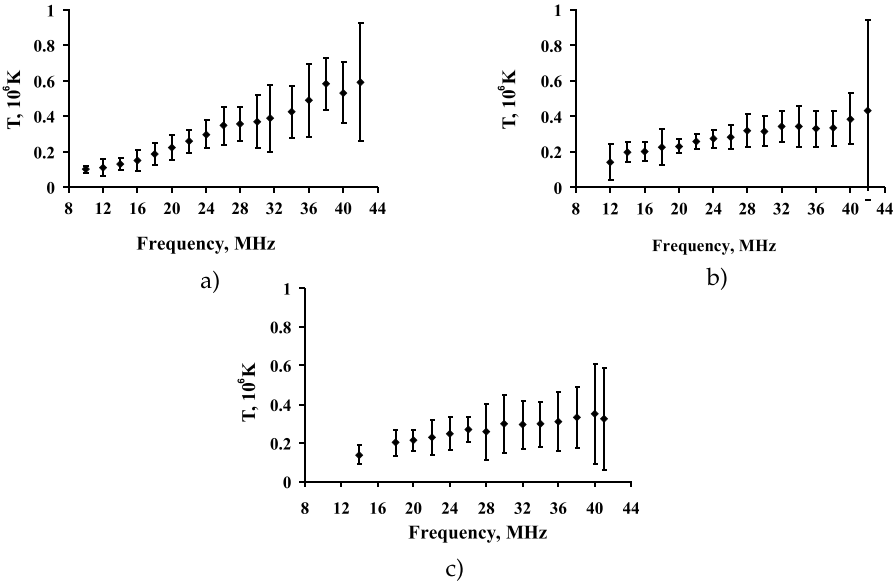

Figure 12 The dependencies of the temperature on frequency for all three temporal intervals.

time, then knowing the durations of the spikes at different frequencies enables building of the profile of the coronal temperature *versus* height above the solar surface.

3.2. Spikes Bandwidth

Spikes have a narrow frequency bandwidth, which depends on the frequency. In contrast to the temporal profile, the frequency profile of spikes is symmetrical (see Figure 6). The average value of the decameter spike bandwidth grows with the frequency, from 25 ± 5.8 kHz at frequency 11 MHz to 80 ± 17.2 kHz at frequency 40 MHz, which is approximately 0.2 %

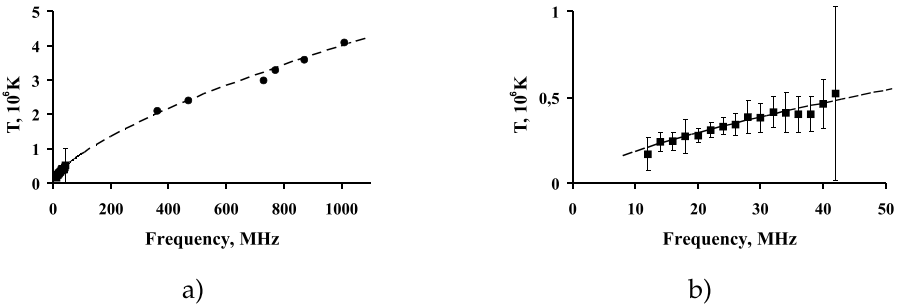

Figure 13 The dependence of the temperature on the frequency. The dashed line corresponds to those obtained empirically; while the circles correspond to the data obtained by Guedel *et al.* (1990), and the squares correspond to the data that we obtained for the second time interval.

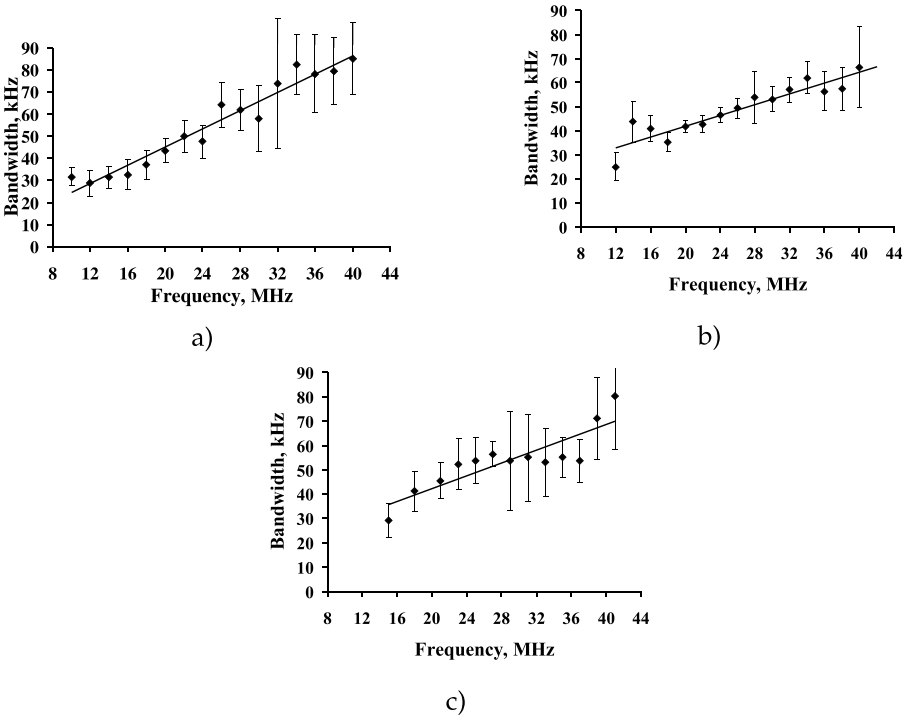

Figure 14 The dependencies of the spike bandwidth on the frequency for all three temporal intervals.

of the central frequency. The dependencies of the bandwidth on the frequency for all three time intervals are presented in Figure 14.

Similar to Melnik *et al.* (2014), these dependencies were (least squares) approximated by linear functions, *i.e.* in the form:

$$\Delta f \propto Af. \tag{4}$$

The values of the coefficients A are presented in Table 3.

Table 3 The values of coefficient of proportionality [A] and angle [θ]

	Temporal interval		
	I	II	III
A	2.1×10^{-3}	1.1×10^{-3}	1.3×10^{-3}
$\theta(B = 2\,\mathrm{G})$	17°	12°	13°

According to the ideas and the assumptions proposed by Melnik *et al.* (2014), we assume that the fast electron beams propagating through the plasma are responsible for the generation of spikes. These fast electrons propagate in some solid angle [θ] and excite Langmuir waves [l] at the upper hybrid frequency. These Langmuir waves [l] are scattered on ions [i] in a process [$l + i \rightarrow t + i$], and as a result they are transformed into electromagnetic waves [t] at a frequency that is approximately equal to the local plasma frequency [ω_{pe}]. In the case when $\omega_{\mathrm{Be}} \ll \omega_{\mathrm{pe}}$, the bandwidth of these waves is given by

$$\Delta\omega = \omega_{\mathrm{uh}}(\theta) - \omega_{\mathrm{uh}}(0) \approx \frac{\omega_{\mathrm{Be}}^2}{2\omega_{\mathrm{pe}}} \sin^2\theta. \tag{5}$$

When we rewrite Equation (5) as a ratio of the frequency bandwidth and the central frequency:

$$\frac{\Delta f}{f} = \frac{\omega_{\mathrm{Be}}^2}{2\omega_{\mathrm{pe}}^2} \sin^2\theta, \tag{6}$$

and we compare it with the experimentally found dependence in Equation (4), we can obtain an expression for the angle θ in which the beam of electrons is confined:

$$\theta = \arcsin\left(\sqrt{2A}\frac{\omega_{\mathrm{pe}}}{\omega_{\mathrm{Be}}}\right), \tag{7}$$

where $\omega_{\mathrm{pe}} = \sqrt{4\pi e^2 n/m}$ denotes the plasma frequency, $\omega_{\mathrm{Be}} = eB/mc$ corresponds to the electron-cyclotron frequency, and B is the magnetic field. If we assume that the magnetic field [B] is about 2 G at the distance that corresponds to the decameter range (Melnik *et al.*, 2010a), then the angle θ is changing from 12° to 17° for the observed values of A (Table 3). We note that these obtained values of θ are in good agreement with the estimates obtained by Zaitsev (1975) and by Melnik *et al.* (2014).

On the other hand, if we assume that the electron beam responsible for generation of spikes is confined to some average solid angle ($\theta = 15°$), and knowing the coefficients A, we can determine the magnetic field [B] along the electron-beam path. This yields, for example, the result that the magnetic field of the ambient plasma during the second temporal interval amounts to about 1.6 G.

Also it is necessary to draw attention to Figure 14c, which shows the third time interval, in which spikes are superposed on the Type IV continuum. It can be seen that at frequencies 28 – 38 MHz a small decrease of bandwidth is observed. This decrease is probably associated with magnetic-field inhomogeneities at the corresponding heights.

3.3. Flux

Generally the decameter spike fluxes do not exceed 500 s.f.u. and in most cases they are even below 100 s.f.u. (Melnik *et al.*, 2014).

The distributions of spike fluxes are presented in Figure 15. The majority of bursts occur in the range from 20 s.f.u. to 100 s.f.u. with the largest number of bursts occurring with

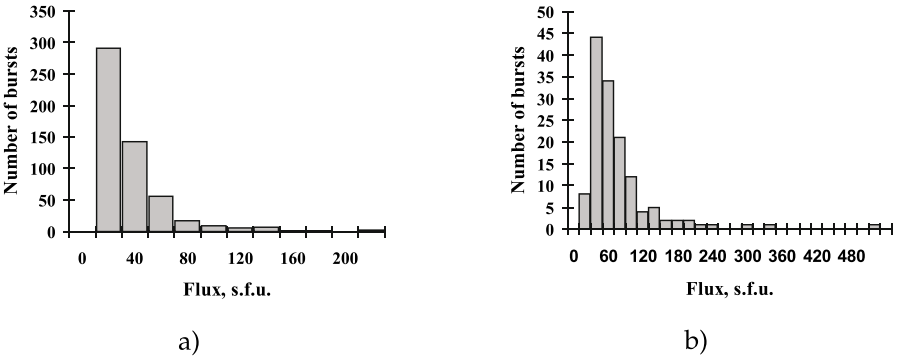

Figure 15 The flux-distribution histograms for the second (a) and third (b) intervals.

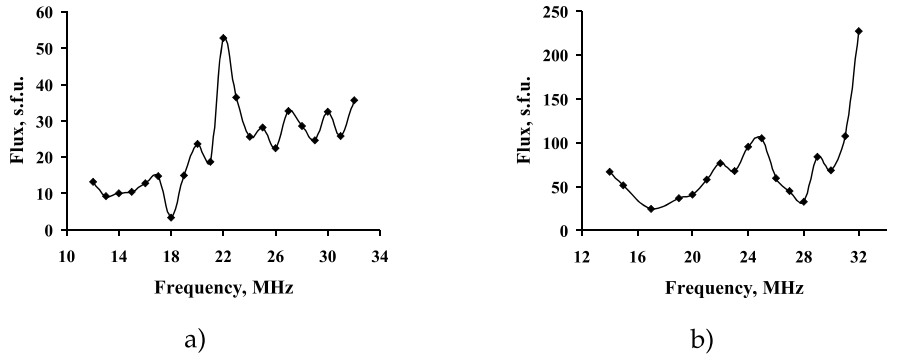

Figure 16 Spike-flux dependences on frequency for the second (a) and third (b) time intervals.

fluxes of 20 – 40 s.f.u. The bursts with fluxes larger than 100 s.f.u. are rare. The maximum value of the flux registered on this day is 520 s.f.u.

Dependence of the average flux on the observing frequency, for the second and third time interval, is shown in Figure 16. We did not find any dependence of the average flux on the observing frequency, similar to results obtained by Melnik *et al.* (2014).

According to Messerotti, Nonino, and Zlobec (1985) and Benz (1986), the brightness temperature [T_b] of decimeter spikes is in the range $10^{12} - 10^{15}$ K. Such high values of T_b can be achieved only as a result of a coherent mechanism of radiation.

We used the Rayleigh–Jeans law for the flux to derive the expression for the brightness temperature of radiation (Kraus, 1966):

$$T_b = \frac{Ic^2}{2k_B \Omega f^2}, \tag{8}$$

where I corresponds to the flux, c denotes the speed of light, k_B is the Boltzmann constant, f denotes the observational frequency, and Ω is the angular size of the radiation source.

According to Abranin *et al.* (1978), the angular size of the sources of stria bursts have apparent diameters between 20′ and 50′ at the frequency 25 MHz. These values do not differ noticeably from those obtained for decameter Type III bursts (Abranin *et al.*, 1978; Dulk and Suzuki, 1980; Gopalswamy and Kundu, 1987). In the decameter range, the parameters

of striae (*i.e.* their duration, bandwidth, and flux) are practically the same as the parameters of spikes (Melnik *et al.*, 2010b). Hence, it is reasonable to assume that the sizes of their sources are also more or less the same. Assuming that the radiation is isotropic and escapes from a spherical source, we obtained brightness temperatures of spike bursts in the range $10^9 - 10^{10}$ K . These brightness temperatures indicate that the mechanism of the spikes generation is non-thermal and, in our case, it is likely to be plasma emission.

4. Conclusions

In this article we analyzed the event observed on 14 June 2012, in the frequency range 8 – 42 MHz. On this day, a storm of spikes concurrent with Type III bursts storm and a Type IV continuum was recorded.

In this extensive study, radio spikes are used not only as a tool for determination of the coronal-plasma parameters but also for tracing the changes of the temperature $[T]$ and the magnetic field $[B]$ in the course of the day. We assumed that the spikes duration is comparable with the collision time of particles in plasma and that the frequency bandwidth is determined by the magnetic field at a certain heights.

According to our analysis, the coronal temperature decreases during the day of observations. As a matter of fact, during the first temporal interval the coronal temperature at the heights 3.3 – 1.6 solar radii (using Newkirk's empirical coronal model) was $\approx 0.1 - 0.6 \times 10^6$ K. During the second and third time intervals the temperature estimated at the heights 2.9 – 1.6 solar radii was found to be $\approx 0.2 - 0.43 \times 10^6$ K and $\approx 0.13 - 0.32 \times 10^6$ K, respectively. We noticed that the coronal temperatures obtained with this method are considerably lower than the commonly known value of about 10^6 K at coronal heights which correspond to the decameter wavelength range. However, according to the assumption made by Elgaröy and Eckhoff (1966) we may assume that spikes similar to the fine structured meter Type I bursts may possibly be generated in "cold" filaments.

In this study we also found that the spike bandwidth is linearly increasing with the observational frequency, and the coefficient $[A]$ (see Equation (4)) equals 2.1×10^{-3}, 1.1×10^{-3}, 1.3×10^{-3} for the first, second, and third temporal intervals, respectively.

If we assume that the electron beam responsible for the generation of the spikes propagates within some average angle $\theta = 15°$ (Zaitsev, 1975), then the value of the magnetic field strength $[B]$ varies in the range 1.6 – 2 G during the day. The magnetic field herein obtained is also in good agreement with the results obtained by other authors, *e.g.* Melnik *et al.* (2010a, 2014). All of these findings indicate that the magnetic field is not varying too much in the decameter frequency range.

The comparison of temporal characteristics of decameter spikes studied herein with those characteristics of the high-frequency spikes (Guedel and Benz, 1990) indicates that we most likely are considering the same family of solar radio bursts.

Acknowledgements The work was partially fulfilled in the framework of FP7 project SOLSPANET (FP7-PEOPLE-2010-IRSES-269299) and by project DBOF-12-0261 of the KU Leuven.

Disclosure of Potential Conflicts of Interest The authors declare that they have no conflicts of interest.

References

Abranin, E.P., Bazelian, L.L., Goncharov, N.I., Zaitsev, V.V., Zinichev, V.A., Rapoport, V.O., Tsybko, I.G.: 1978, Angular sizes of stria-burst sources in the range 24 – 26 MHz. *Solar Phys.* **57**, 229. DOI. ADS.

Bakunin, L.M., Chernov, G.P.: 1985, Broadband solar bursts of the spike type. *Soviet Astron.* **29**, 564. ADS.
Barrow, C.H., Saunders, H.: 1972, Fast polarized pulses in decameter-wave radiation from the Sun. *Astrophys. J. Lett.* **12**, 211. ADS.
Baselian, L.L., Goncharov, N.I., Zaitsev, V.V., Zinichev, V.A., Rapoport, V.O., Tsybko, I.G.: 1974, Frequency and time splitting of decameter solar radio bursts. I – Elementary events. *Solar Phys.* **39**, 213. DOI. ADS.
Benz, A.O.: 1986, Millisecond radio spikes. *Solar Phys.* **104**, 99. DOI. ADS.
Benz, A.O., Csillaghy, A., Aschwanden, M.J.: 1996, Metric spikes and electron acceleration in the solar corona. *Astron. Astrophys.* **309**, 291. ADS.
Benz, A.O., Su, H., Magun, A., Stehling, W.: 1992, Millisecond microwave spikes at 8 GHz during solar flares. *Astron. Astrophys. Suppl. Ser.* **93**, 539. ADS.
Boischot, A., Rosolen, C., Aubier, M.G., Daigne, G., Genova, F., Leblanc, Y., Lecacheux, A., de La Noe, J., Moller-Pedersen, B.: 1980, A new high-gain, broadband, steerable array to study Jovian decametric emission. *Icarus* **43**, 399. DOI. ADS.
Braude, S.Y., Men', A.V.: 1996, Radio astronomy researches in Ukraine in decameter wave range. *Radio Phys. Radio Astron.* **1**, 9.
Dąbrowski, B.P., Rudawy, P., Karlický, M.: 2011, Millisecond radio spikes in the decimetric band. *Solar Phys.* **273**, 377. DOI. ADS.
De Groot, T.: 1960, Dynamic spectra and polarization of small bursts in solar radio emission. *Bull. Astron. Inst. Neth.* **15**, 229.
de La Noe, J.: 1975, Spectral characteristics of stria, split pair and triple bursts. *Astron. Astrophys.* **43**, 201. ADS.
Droege, F.: 1977, Millisecond fine-structures of solar burst radiation in the range 0.2 – 1.4 GHz. *Astron. Astrophys.* **57**, 285. ADS.
Dulk, G.A., Suzuki, S.: 1980, The position and polarization of Type III solar bursts. *Astron. Astrophys.* **88**, 203. ADS.
Elgaröy, Ö.: 1961, Studies in high-resolution spectrometry of solar radio emission. *Astrophys. Nor.* **7**, 123.
Elgaröy, Ö.: 1967, On the wavelength dependence of the bandwidth and the duration of type I solar radio bursts. *Astrophys. J. Lett.* **1**, 13. ADS.
Elgaröy, Ö., Eckhoff, H.K.: 1966, On the active region corona and the interpretation of type I burst. *Astrophys. Nor.* **10**, 127. ADS.
Ellis, G.R.A., McCulloch, P.M.: 1967, Frequency splitting of solar radio bursts. *Aust. J. Phys.* **20**, 583. ADS.
Fleishman, G.D., Mel'nikov, V.F.: 1998, Millisecond solar radio spikes. *Phys. Usp.* **41**, 1157. DOI. ADS.
Gopalswamy, N., Kundu, M.R.: 1987, Imaging observations of the evolution of meter-decameter burst emission during a major flare. *Solar Phys.* **111**, 347. DOI. ADS.
Guedel, M., Benz, A.O.: 1990, Time profiles of solar radio spikes. *Astron. Astrophys.* **231**, 202. ADS.
Kraus, J.D.: 1966, *Radio Astronomy*, Cygnus-Quasar, Powell, OH. ADS.
Markeev, A.K., Chernov, G.P.: 1970, Observations of solar radio bursts with high spectral resolution. *Astron. Zh.* **47**, 1044. ADS.
McKim Malville, J., Aller, H.D., Jensen, C.J.: 1967, Spike bursts during the type IV event of February 5, 1965. *Astrophys. J.* **147**, 711. DOI. ADS.
Megn, A.V., Sharykin, N.K., Zaharenko, V.V., Bulatsen, V.G., Brazhenko, A.I., Vaschishin, R.V.: 2003, Decameter wavelength radio telescope URAN-2. *Radio Phys. Radio Astron.* **8**, 345.
Melnik, V.N., Konovalenko, A.A., Rucker, H.O., Dorovskyy, V.V., Abranin, E.P., Lecacheux, A., Lonskaya, A.S.: 2010a, Solar S-bursts at frequencies of 10 – 30 MHz. *Solar Phys.* **264**, 103. DOI. ADS.
Melnik, V.N., Rucker, H.O., Konovalenko, A.A., Shevchuk, N.V., Abranin, E.P., Dorovskyy, V.V., Lecacheux, A.: 2010b, Type IIIb bursts and their fine structure in frequency band 18 – 30 MHz. In: Chakrabarti, S.K., Zhuk, A.I., Bisnovatyi-Kogan, G.S. (eds.) **CP-1206**, AIP, Melville, 445. DOI. ADS.
Melnik, V.N., Shevchuk, N.V., Konovalenko, A.A., Rucker, H.O., Dorovskyy, V.V., Poedts, S., Lecacheux, A.: 2014, Solar decameter spikes. *Solar Phys.* **289**, 1701. DOI. ADS.
Messerotti, M., Nonino, M., Zlobec, P.: 1985, Polarization and brightness temperature of 'spike' bursts related to metric Type IV solar radio events. *Mem. Soc. Astron. Ital.* **56**, 795. ADS.
Ryabov, V.B., Vavriv, D.M., Zarka, P., Ryabov, B.P., Kozhin, R., Vinogradov, V.V., Denis, L.: 2010, A low-noise, high-dynamic-range, digital receiver for radio astronomy applications: An efficient solution for observing radio-bursts from Jupiter, the Sun, pulsars, and other astrophysical plasmas below 30 MHz. *Astron. Astrophys.* **510**, A16. DOI. ADS.
Sawant, H.S., Bhonsle, R.V., Alurkar, S.K.: 1976, Microscopic spectral features in solar decametric bursts and coronal irregularities. *Solar Phys.* **50**, 481. DOI. ADS.
Stewart, R.T.: 1975, An example of a fundamental type IIIb radio burst. *Solar Phys.* **40**, 417. DOI. ADS.
Takakura, T.: 1959, Polarized bursts and noise storms of solar radio emission. II. Storm bursts and background continuum. *Publ. Astron. Soc. Japan* **11**, 55. ADS.
Tarnstrom, G.L., Philip, K.W.: 1972, Solar radio spike bursts. *Astron. Astrophys.* **16**, 21. ADS.

Warwick, J.W., Dulk, G.A.: 1969, Spectrum and polarization of solar radio bursts on a 10-millisecond time scale. *Astrophys. J. Lett.* **158**, L123. DOI. ADS.

Weber, R., Viou, C., Coffre, A., Denis, L., Zarka, P., Lecacheux, A.: 2005, DSP-enabled radio astronomy: Towards IIIZW35 reconquest. *EURASIP J. Appl. Signal Process.* **16**, 2686.

Zaitsev, V.V.: 1975, Quasi-one-dimensionality of plasma wave spectrum in type III radio burst sources. *Soviet Astron.* **18**, 475. ADS.

Zhelezniakov, V.V., Zaitsev, V.V.: 1975, Some features of solar spike burst generation. *Astron. Astrophys.* **39**, 107. ADS.